Physiologically Structured Models of Rotifer Population Dynamics in a Chemostat

James N. McNair
Grand Valley State University
Annis Water Resources Institute
740 West Shoreline Drive
Muskegon, MI 49441

1 Introduction

Current knowledge of the principles of population dynamics is unsatisfactory on both empirical and theoretical grounds. The main problems are a weak empirical base, overly simple models with but vague links to real systems, and little effective interplay between theory and experiment. We therefore believe there is a need for renewed emphasis on carefully controlled laboratory studies of population dynamics, and on the development of structured population models that can be related clearly, directly, and convincingly to real experimental systems.

The rotifer chemostat is an excellent system for conducting laboratory population-dynamics studies. Relevant experimental techniques, concepts, and sample data are outlined by Boraas et al. (1998). Here we summarize the basic ideas underlying classical models of the chemostat, show that these models are inadequate for rotifers, and outline an alternative modeling approach that we believe has the potential to provide a more satisfactory theory. Additional discussion can be found in the paper by McNair et al. (1998), on which the present document is based.

2 Classical Chemostat Models

The main component of the rotifer chemostat is an enclosed culture vessel containing a suspension of rotifers and algae (Figure 1). The culture is kept well mixed to maintain spatial homogeneity. Fresh algal suspension (from an algal chemostat) is pumped into the culture at a continuous, regulated rate. Since the culture volume is fixed, outflow exactly balances inflow (dimensions: volume $\cdot$ time^{-1}). The culture vessel is kept in the dark (to prevent any significant algal growth or division) under tightly controlled physical conditions and is monitored regularly (see Boraas et al., 1998, for additional details). In attempting to characterize the rotifer chemostat mathematically, previous studies have employed models originally developed for unicellular organisms, including Monod's (1950) model and a few straightforward variants. We refer to these collectively as classical chemostat models. A typical example is the Monod-Herbert model (Herbert, 1958), which differs from Monod's model simply by permitting loss of biomass via catabolism.

All classical chemostat models assume that the state of a rotifer population at any time t can be adequately characterized by a single number $M(t)$, which usually is some measure of the total mass of the population (e.g., total carbon). The dynamics of $M(t)$ are assumed to be determined by the difference between the rate at which total rotifer biomass grows (as a result of ingesting algae and converting it into rotifer biomass) and the rates at which total rotifer biomass is diminished by

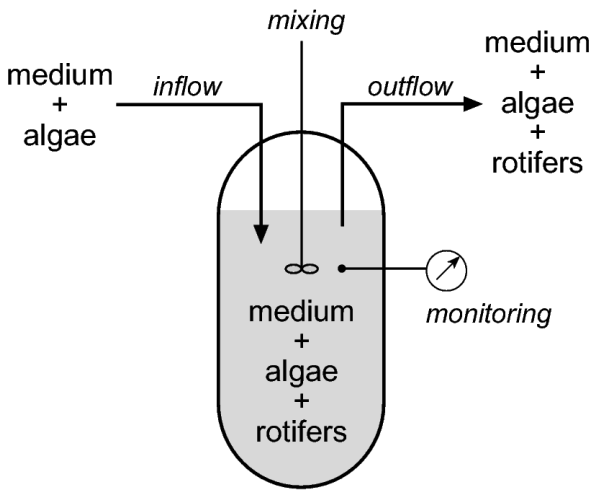

Figure 1. Basic components of the rotifer chemostat (highly schematic). See text for description, and Boraas et al. (1998) for additional details.

catabolism and mortality and by being washed out of the chemostat. Similarly, it is assumed that the state of the algae population can be adequately characterized by a single number representing its total mass, whose dynamics are determined by the difference between the rate at which algal biomass is fed into the chemostat and the rates at which it is removed by rotifer ingestion and by being washed out of the system. Equations governing the states of the algae and rotifer populations are usually stated in terms of the respective mass concentrations A(t) and R(t); e.g., $R(t) = M(t)/V$, where V is the (constant) culture volume. The Monod-Herbert model, for example, can be written in the form,

$$\begin{aligned} \frac{\mathrm{d}A}{\mathrm{d}t} &= A_0 D - AD - \frac{I_{sup} AR}{K_h + A} \\ \frac{\mathrm{d}R}{\mathrm{d}t} &= Y \frac{I_{sup} AR}{K_h + A} - \rho R - DR, \end{aligned} \tag{1}$$

where the first and second equations specify the instantaneous rates of change in mass concentrations of algae and rotifers, respectively. Variables and parameters (with dimensions) are as follows:

$A(t)$ = algal mass concentration in the culture at time t [mass $\cdot$ volume^{-1}]
$R(t)$ = rotifer mass concentration in the culture at time t [mass $\cdot$ volume^{-1}]
A_0 = algal mass concentration in the feed [mass $\cdot$ volume^{-1}]
K_h = half-saturation constant for ingestion [mass $\cdot$ volume^{-1}]
D = dilution rate (inflow Q divided by culture volume V) [time^{-1}]
I_{sup} = asymptotic mass-specific rate of ingestion by rotifers [time^{-1}]
ρ = mass-specific rate of mortality and metabolic loss of rotifer biomass [time^{-1}]
Y = yield coefficient (rotifer mass produced per unit algal mass ingested) [dimensionless].

The three terms on the right side of the algae equation correspond to algal input, washout, and ingestion by rotifers. The three terms on the right side of the rotifer equation correspond to production of rotifer biomass from ingested algae, mortality and metabolic loss of biomass, and

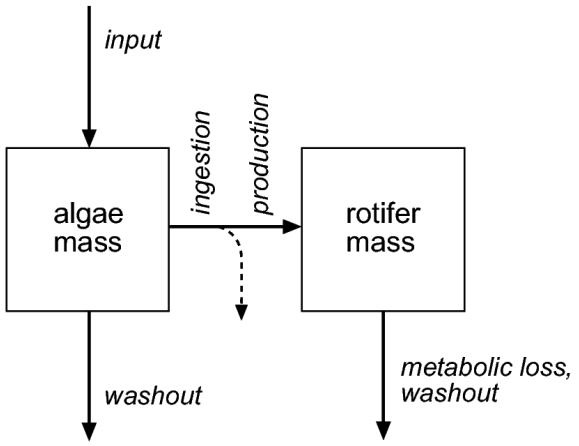

Figure 2. Schematic of the Monod-Herbert model. See text for description.

washout. The model is shown schematically in Figure 2. It is important to note that equations (1) assert that the dynamics of algal and rotifer mass can be understood and predicted with no knowledge of the internal structure of either population (e.g., age or size structure). Thus, according to equations (1), if we set up a chemostat with fixed initial masses of algae and rotifers, it should make no difference to the system's short-term dynamics whether the rotifer population consists entirely of eggs (which would not ingest algae, and would neither reproduce nor increase in dry mass), entirely of gravid females (which would ingest algae, reproduce, and possibly increase in dry mass, as well), or of some mix of life stages. If this property were to hold for real rotifer chemostats, it would be a most remarkable one, indeed.

3 Key Experimental Evidence

We now show results of several experiments that permit an assessment of classical chemostat models, here represented by the Monod-Herbert model. Figure 3A shows the results of an experiment conducted by Boraas (1983) in which *Brachionus calyciflorus* was introduced into a chemostat at low abundance and allowed to grow. Figure 3B shows the dynamics predicted by a calibrated Monod-Herbert model. Note the contrast between the smooth approach to steady state predicted by the model and the pronounced and persistent fluctuation observed. This result is typical of such experiments (e.g., Rothaupt, 1993; Walz, 1993) and reveals that the Monod-Herbert model exhibits too little tendency toward oscillation, compared to real rotifer populations. (Oscillation becomes far more pronounced if algae are allowed to grow, but the cause of oscillation is quite different than in the case where algal growth is prohibited.)

A more striking discrepancy is demonstrated in Figure 4, which shows the results of a downward D-shift experiment conducted by Boraas (1983). The chemostat was allowed to run for roughly 1000 h at $D = 0.045$ h^{-1}, after which D was abruptly decreased to 0.0135 h^{-1} (by reducing the pump speed). As the figure shows, the observed transient dynamics following the downward shift in D (panel A) bear little resemblance to the behavior predicted by the calibrated Monod-Herbert model (panel B). Most notably, the algae showed a dramatic resurgence following their initial crash, whereas the model predicted essentially none. A similarly gross discrepancy was observed by Walz

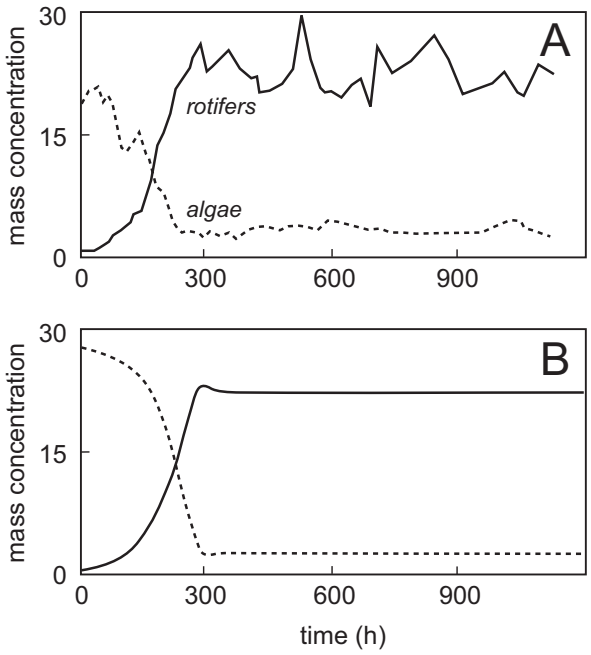

Figure 3. Examples of rotifer (*Brachionus calyciflorus*) chemostat dynamics in laboratory experiments. A—Approach to quasi-steady state. Mass concentration units: $\mu g \cdot mL^{-1}$ for rotifers, $\mu g \cdot mL^{-1} \times 5.7$ for algae. B—Dynamics predicted by the Monod-Herbert model for data series A. Units: same as in A. Data: Boraas (1983).

(1993) in a D-shift experiment with *Brachionus angularis*.

Another serious problem with classical chemostat models as applied to rotifers is that they are unable to address phenomena dealing with population structure. For example, panels A and B of Figure 5 (redrawn from Boraas, 1983) show dynamics of the rotifer size structure corresponding to the mass dynamics in Figures 3A and 4A. In panel B, note that the D shift is followed by loss of the egg peak, accumulation of juveniles and small adults, then return of the egg peak (egg, juvenile, and adult segments of the size distribution are identified in Figure 6). Another example appears in Figure 6 (from Bennett & Boraas, 1989), which shows the steady-state rotifer size distribution at three different dilution rates. Note that the steady-state egg peak is taller relative to the adult peak at higher dilution rates. Size-structure patterns such as these provide valuable clues about the mechanisms of rotifer population regulation but cannot be addressed using classical models.

Based on the inability of classical chemostat models to account for observed transient dynamics of total mass, and on their inability to address observed patterns in population structure (and also for theoretical reasons beyond the scope of this brief presentation), we believe that these models are inadequate tools for studying the rotifer chemostat. In the next section, we propose a new modeling approach that resolves some of these problems.

4 A Simple Physiologically Structured Model

Our objective in developing a new model of the rotifer chemostat was to add the minimum biological detail necessary to account for currently known phenomena, and to increase the correspondence

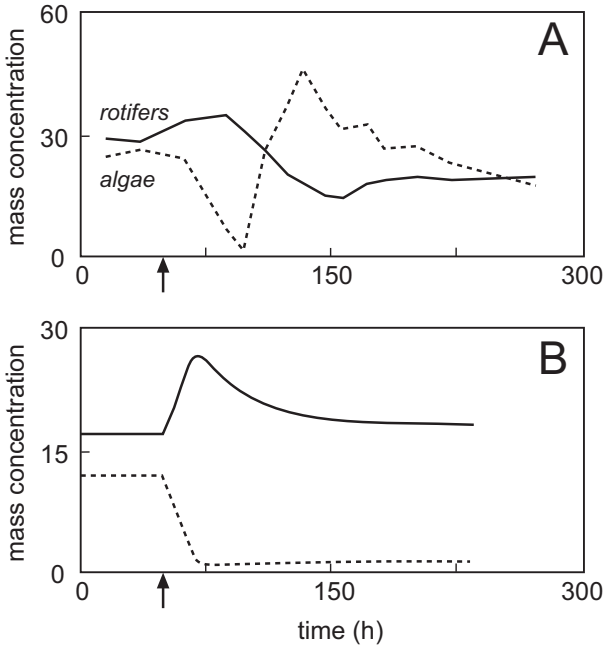

Figure 4. Examples of rotifer (*Brachionus calyciflorus*) chemostat dynamics in laboratory experiments. A—Effect of a downward shift in dilution rate (arrow) following the end of the data series shown in Figure 3A. Units: $\mu g \cdot mL^{-1}$ for rotifers and algae. B—Dynamics predicted by the Monod-Herbert model for the data series in panel A. Units: same as in A. Data: Boraas (1983).

between model components and experimentally measurable properties. We therefore decided to (a) add only a few key components of structure to the rotifer population, (b) focus on structural components that are experimentally measurable and directly related to basic physiological mechanisms, (c) keep the model simple enough so it is both computationally tractable and reasonably transparent to underlying principles, and (d) pose the model in a form that can be reduced to a classical model via specializing assumptions (so the reasons for differences in model properties can be clearly identified).

The basic idea behind the model is illustrated in Figure 7. Recall from Figure 2 that classical chemostat models can be diagramed as two (connected) boxes with no internal structure. We retain the algae box of the classical model but add two types of structure to the rotifer box. First, the population is divided into two discrete stages: eggs and free-swimming rotifers (hereafter, rotifers). Second, each stage is given a different type of continuous internal structure: generalized age for eggs (e.g., degree days) and body mass for rotifers. Thus, the new model is only slightly more complex than classical models and remains biologically quite simple.

The model works as follows. Rotifers continuously ingest algae and consequently grow along the body mass axis (with negative growth allowed). Once a threshold body mass is crossed, they become adults and begin allocating some of their net assimilated mass to egg production. The eggs produced enter the age axis of the egg stage at generalized age 0 and begin a process of development, eventually crossing a threshold age at which they begin to hatch. The neonates produced return to the body mass axis of the rotifer stage, with variability in neonatal body size allowed. The newborn rotifers then begin to grow, and the life cycle is complete.

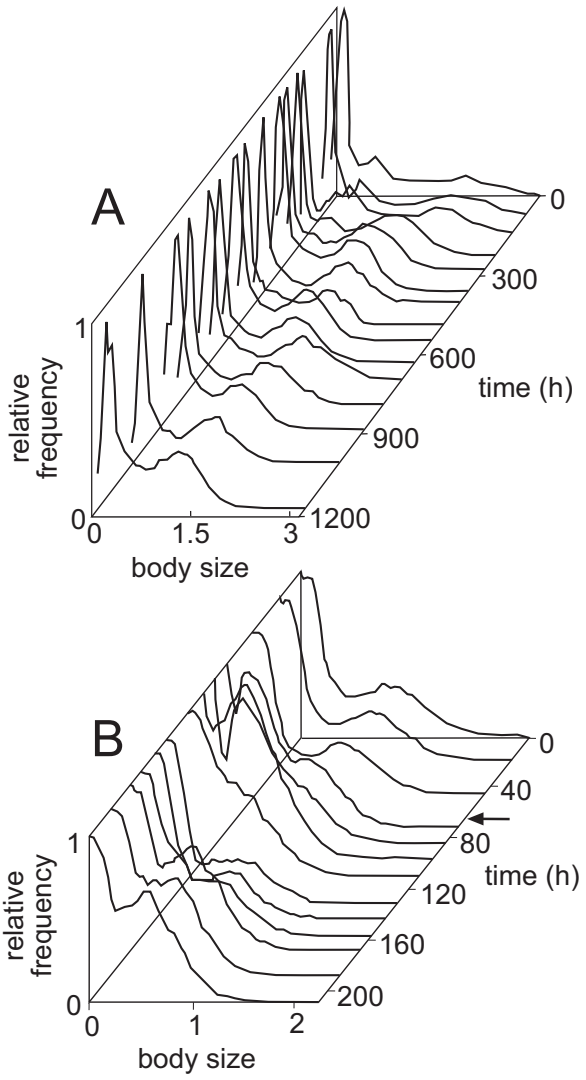

Figure 5. Observed dynamics of the rotifer size distribution in the data series shown in Figures 3A and 4A. Size distributions are normalized to achieve a constant egg-peak height; non-normalized distributions are shown in Figure 5 of Boraas et al. (1998). Body size units: $\mu\text{m}^3 \times 10^6$. Data: Boraas (1983).

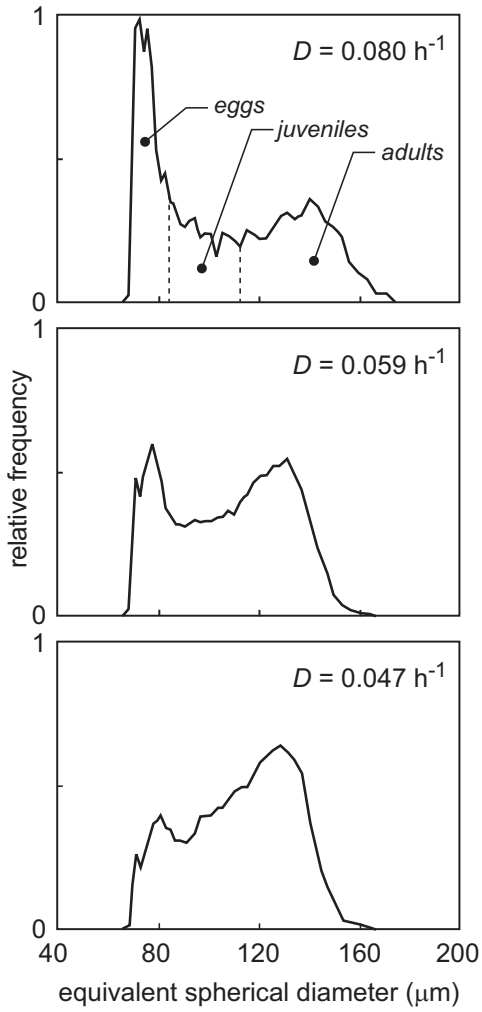

Figure 6. Steady-state rotifer size distributions at three different dilution rates. Top distribution shows approximate sizes of eggs, juveniles, and adults. Data: Bennett & Boraas (1989).

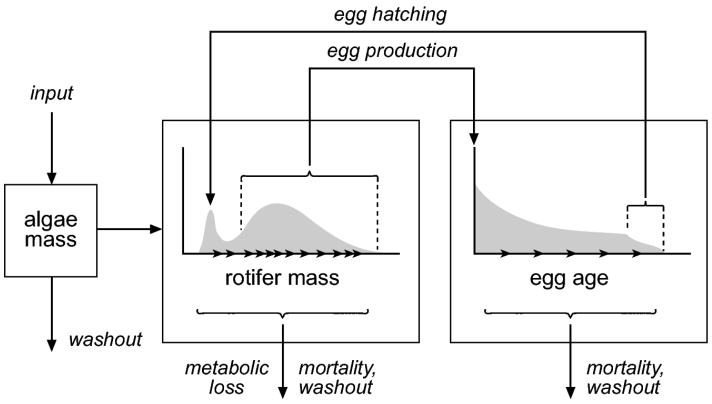

Figure 7. Schematic of the physiologically structured chemostat model. See text for description.

Using the methods of continuum transport modeling, the schematic of Figure 7 is easily translated into a set of equations comprising an ordinary differential equation governing the algae, a mass-structured hyperbolic partial differential equation (with boundary condition) governing the rotifers, and an age-structured hyperbolic partial differential equation (with boundary condition) governing the eggs:

$$\begin{aligned}
\frac{\mathrm{d}A}{\mathrm{d}t} &= (A_0 - A)D - \varepsilon \int_{x_0}^{\infty} F(A,x)n(t,x)\mathrm{d}x \\
\frac{\partial n}{\partial t} + \frac{\partial(\gamma n)}{\partial x} &= b(x)\int_0^{\infty} \nu(a)n_e(t,a)\mathrm{d}a - [\mu(A,x) + D]n(t,x), \quad x > x_0 \\
&\quad \text{subject to } n(t,x_0) = 0 \text{ when } \gamma(A,x_0) > 0 \\
\frac{\partial n_e}{\partial t} + u\frac{\partial n_e}{\partial a} &= [\nu(a) + \mu_e(a) + D]n_e(t,a), \quad a > 0 \\
&\quad \text{subject to } un_e(t,0) = \int_{x_0}^{\infty} \beta(A,x)n(t,x)\mathrm{d}x,
\end{aligned} \tag{2}$$

where

$A(t)$ = total mass of algae at time t, per unit volume of culture
$n(t,x)\mathrm{d}x$ = number of rotifers with body mass between x and $x + \mathrm{d}x$ at time t, per unit volume of culture
$n_e(t,a)\mathrm{d}a$ = number of eggs with generalized age between a and $a + \mathrm{d}a$ at time t, per unit volume of culture
$\gamma(A,x)$ = rate of growth in rotifer body mass at body mass x
$b(x)$ = probability density function for the mass of a rotifer egg
$\nu(a)$ = egg maturation rate at generalized age a
$\mu(A,x)$ = mortality rate of rotifers at body mass x
D = dilution rate
u = temperature-dependent rate of generalized aging in eggs
$\mu_e(a)$ = egg mortality rate at generalized age a
A_0 = input mass concentration of algae
ε = algal cell mass
$F(A,x)$ = rotifer ingestion rate at body mass x (cells per time per rotifer)
x_0 = lower limit of body mass for a rotifer
$\beta(A,x)$ = rotifer egg production rate at body mass x.

Other choices of the boundary condition for the rotifer equation are plausible. All quantities except γ are restricted to being nonnegative, and we assume $b(x) > 0$ for $x_1 < x < x_2$, and $b(x) = 0$ otherwise (so all egg masses fall within a finite interval).

The rates at which eggs and rotifers are transported along their respective structural axes are determined by the rates of generalized aging and of growth in body mass. For simplicity, we assume in the numerical examples below that generalized aging occurs at a constant rate $u = 1$, which is equivalent to chronological aging. Growth in body mass is assumed to be given by the amount of net assimilation (gross assimilation minus metabolic loss) allocated to growth rather than reproduction. The net assimilation rate $\alpha(A, x)$ is given by

$$\alpha(A, x) = [\varepsilon p(A, x) - \xi(A, x)]F(A, x) - \rho x^\theta,$$

where $p(A, x)$ is the assimilation fraction, $\xi(A, x)$ is assimilate spent on acquisition and processing per ingested cell, and ρx^θ is the resting metabolic loss rate. Growth and fecundity are then given by

$$\begin{aligned} \gamma(A, x) &= \alpha(A, x)\phi_s(\alpha, x) \\ \beta(A, x) &= \frac{\alpha(A, x)\phi_r(\alpha, x)}{\int yb(y)\mathrm{d}y}, \end{aligned}$$

where $\phi_s(\alpha, x)$ and $\phi_r(\alpha, x)$ are the proportional allocations to somatic growth and reproduction, and the denominator in the formula for $\beta(A, x)$ is the average mass of an egg (which converts reproduction from mass of eggs per time to number of eggs per time). Proportional allocation to somatic growth and reproduction are related by

$$\phi_r(\alpha, x) + \phi_s(\alpha, x) = 1,$$

so it suffices to specify only $\phi_r(\alpha, x)$.

In the numerical examples below, $\phi_r(\alpha, x)$ is assumed to be the product of a component depending only on x and a component depending only on α, with allocation working as follows. No net assimilate is allocated to reproduction if body mass is too small (in which case the size-dependent component is zero) or if net assimilation is too small (in which case the assimilation-dependent component is zero). The size-dependent component is constant except in a certain interval on the body-mass axis (the maturation window) over which it increases from the juvenile value (= 0) to the adult value. The assimilation-dependent component is zero for negative net assimilation and increases toward a positive asymptote with increasing positive net assimilation. These assumptions are for purposes of illustration and probably will require adjustment in actual applications.

5 Numerical Examples

We now provide a few numerical examples to illustrate the behavior of model (2). Figure 8 shows examples of total-mass dynamics. Panels A and B show the initial behavior and approach to steady state with $D = 0.02$ h^{-1} and $D = 0.05$ h^{-1}, respectively. Transient oscillation is evident in A but effectively disappears at high dilution rates, as in B. The dilution rate of example B was shifted downward to $D = 0.02$ h^{-1} at $t = 500$ h, and the subsequent dynamics are shown in panel C. Note that the initial crash in algal mass is followed by a pronounced resurgence, which is roughly the behavior observed by Boraas (1983) and Walz (1993) in their laboratory experiments (e.g., Figure 4A). The assimilation-dependent component of the allocation function plays an important role in determining how pronounced this resurgence is.

Figure 9 shows dynamics of the rotifer size structure during the same numerical experiments whose mass dynamics are shown in the corresponding panels of Figure 8. The size distribution

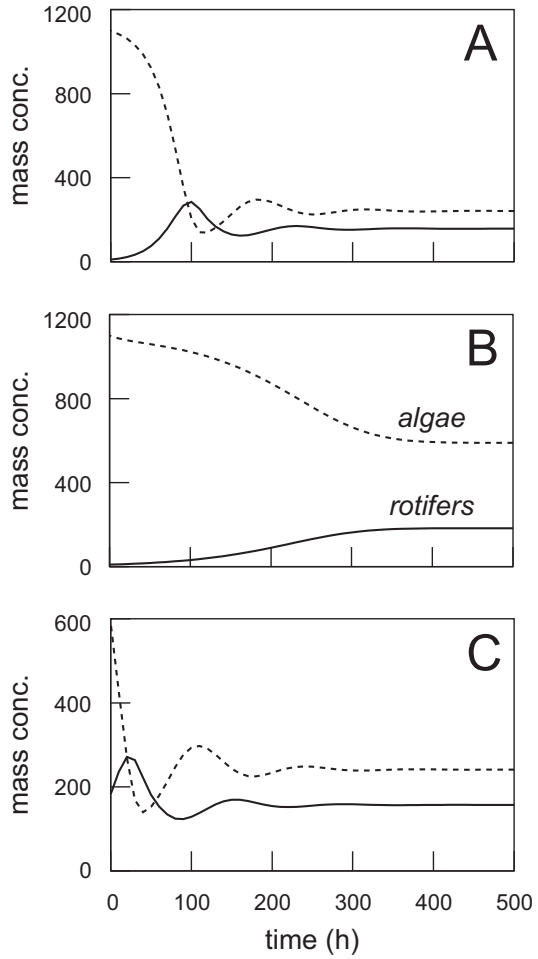

Figure 8. Examples of model total-mass dynamics. A—Total algae and rotifer masses at $D = 0.02$ h^{-1}. B—Total algal and rotifer masses at $D = 0.05$ h^{-1}. C—Continuation of B after a step-change in dilution rate to $D = 0.02$ h^{-1}.

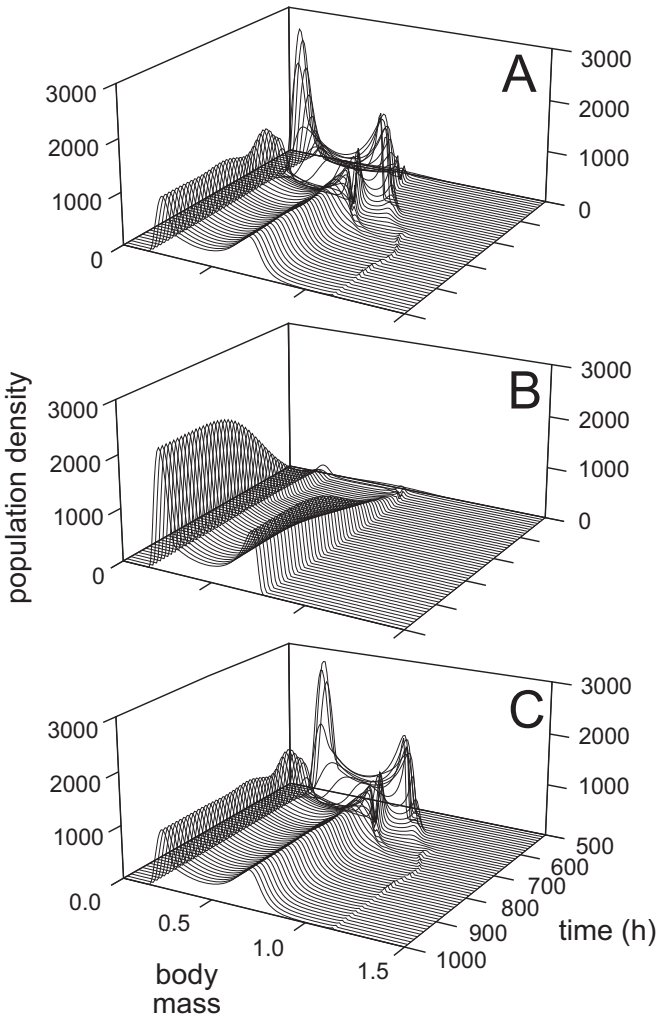

Figure 9. Examples of model size-distribution dynamics. A—Rotifer size distributions corresponding to Figure 8A. B—Rotifer size distributions corresponding to Figure 8B. C—Rotifer size distributions corresponding to Figure 8C.

shows transient wave-like oscillations in panel A, but these disappear at high dilution rates, as in panel B. Similar oscillations are set off by a downward shift in dilution rate, as shown in panel C. Note in particular the initial loss of the egg peak (as the crash in residual algae causes adults to divert net assimilation away from reproduction), the accumulation of juveniles and small adults, then return of the egg peak at a lower height. This is basically the pattern observed by Boraas (1983), shown in Figure 5B above and in Figure 5 of Boraas et al. (1998). Also note that the steady-state egg peak is higher relative to the adult peak when $D = 0.05$ h^{-1} (panel B) than when $D = 0.02$ h^{-1} (panels A, C). This result is consistent with the pattern observed by Bennett & Boraas (1989), shown in Figure 6.

References

Bennett, W.N. & Boraas, M.E. 1989. Comparison of population dynamics between slow- and fast-growing strains of the rotifer *Brachionus calyciflorus* Pallas in continuous culture. *Oecologia* **81**: 494–500.

Boraas, M.E. 1979. *Dynamics of Nitrate, Algae, and Rotifers in Continuous Culture: Experiments and Model Simulations*. Ph.D. thesis, Pennsylvania State University.

Boraas, M.E. 1983. Population dynamics of food-limited rotifers in two-stage chemostat culture. *Limnology and Oceanography* **28**: 546–563.

Boraas, M.E., Seale, D.B., Boxhorn, J.E. & McNair, J.N. 1998. Rotifer size distribution changes during transient phases in open cultures. *Hydrobiologia* **387/388**: 477–482.

Herbert, D. 1958. Some principles of continuous culture. In G. Tunevall (ed.), *Recent Progress in Microbiology*. Blackwell, London: 381–396.

McNair, J.N., Boraas, M.E. & Seale, D.B. 1998. Size-structure dynamics of the rotifer chemostat: a simple physiologically structured model. *Hydrobiologia* **387/388**: 469–476.

Monod, J. 1950. La technique de culture continue; theorie et applications. *Ann. Inst. Pasteur, Lille* **79**: 390–410.

Rothaupt, K.O. 1993. Critical consideration of chemostat experiments. In N. Walz (ed.), *Plankton Regulation Dynamics*. Springer-Verlag, New York: 217–225.

Walz, N. 1993. Model simulations of continuous rotifer cultures. *Hydrobiologia* **255/256**: 165–170.